2014 IEEE/RSJ International Conference on
Intelligent Robots and Systems (IROS 2014)
September 14-18, 2014, Chicago, IL, USA

Optimal Gaits and Motions for Legged Robots

Weitao Xi and C. David Remy, *Member, IEEE*

***Abstract*— In this paper, we explore the potential of trajectory optimization for unspecified contact sequences as a tool to identify optimal gaits and motions for legged robots. This work is based on a recently proposed method that states the mechanical dynamics in a floating base description, makes the ground contact forces part of the free variable vector, and implements the requirement that a foot is either on the ground or that the corresponding contact force is zero via a set of complimentary conditions. We introduce an algorithmic improvement that uses higher order integration for states that are continuous through collisions and thus increases the accuracy of the obtained solutions. The benefits of the proposed changes are evaluated with the models of a 1D hopper and a 2D bipedal robot, and we additionally compare our results with analytic solutions and an established multiple shooting implementation. The proposed method was able to automatically discover walking and running as the most energetically economic ways of locomotion for a conceptual biped that is moving at different speed. It additionally discovers an elastic walking gait that is used at intermediate velocities.**

I. INTRODUCTION

Optimal control is widely used in motion planning for dynamic systems. The general goal is to identify states $\mathbf{y}(t)$ and inputs $\mathbf{u}(t)$ that minimize a cost function C while being subject to additional constraints such as actuator limits, physical restrictions, or periodic boundary conditions. Optimal control methods distinguish themselves primarily in how they transcribe the infinite dimensional problem of optimizing trajectories into a finite dimensional approximation [1]. More advanced methods, such as *multiple shooting* [2] and *direct collocation* [3] utilize parameterized functions with local support for both states and inputs. This parameterization makes it easy to determine a suitable initial guess for the trajectories, leads to problems that are mathematically sparse, and creates well scaled gradients.

In this paper, we consider optimal control problems for multi body systems with intermitted contact. Such problems are essential in the control of legged robots, and we are particularly interested in methods in which the contact sequence is an outcome of the optimization process. The order in which feet strike and leave the ground defines the *gait* of a legged system and has a large impact on performance. To minimize energy consumption, humans –for instance– transit from walking to running as speed increases [4]. A similar effect can be observed in models of bipedal robots [5].

The difficulty of identifying a contact sequence within an optimal control problem arises from the unilateral constraints of ground contact and the collisions that happen when a contact is closed. While these collisions can be modeled with continuous forces created by virtual springs and dampers, the dynamic systems that result from this modelling technique are stiff and ill-suited for numerical integration. Collisions are hence modeled as discrete events with impulsive contact forces and discontinuous velocities. Such hybrid dynamic systems [6] contain both, continuous and discrete dynamics. Since traditional optimal control techniques can only be applied to continuous dynamics, the search for an optimized solution must be restricted to a pre-specified contact sequence; as in the optimization of 3D human like running [7]. Recent advances in trajectory optimization for unspecified contact sequences were obtained by stating the mechanical dynamics in a floating base description and making the ground contact forces part of the free variable vector [8], [9]. Complimentary conditions that state that a foot is either on the ground or that the corresponding contact force is zero are implemented as nonlinear constraints and the resulting problem is solved with direct collocation. Choosing an Euler backward integration scheme in the collocation treats collisions implicitly, and thus allows obtaining results without specifying a contact sequence *a-priory*.

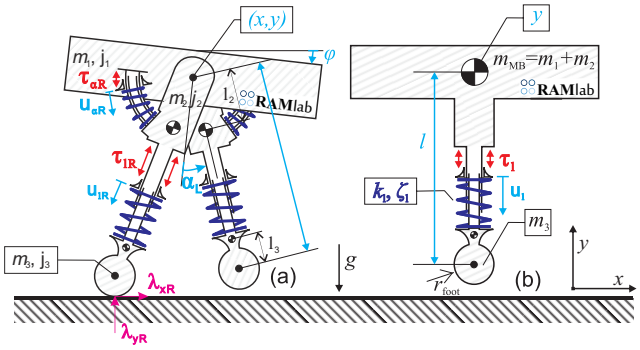

Fig. 1. Optimal gaits and motions were identified for the planar model of a two legged robot (b). The model is driven by series elastic actuators and thus features a rich set of natural dynamics that can be exploited in the locomotion. To quantify the effect of our proposed improvements, a simplified 1D model was used initially (b).

In this paper, we explore the potential of this method to identify different gaits, and propose an improvement that uses higher order integration to increase the precision of the algorithm. To this end, we systematically identify states that are continuous through collisions. We quantify the benefits of the proposed improvements with the models of a 1D hopper and a 2D bipedal robots and compare our results with analytic solutions and an established multiple shooting implementation. Furthermore, we show that a gait transition from *walking* to *running* minimizes energy consumption for a bipedal robot and discover a *elastic walking* gait that is

The authors are with the Robotics and Motion Laboratory (RAMlab), Department of Mechanical Engineering, University of Michigan, Ann Arbor, MI (weitaoxi@umich.edu, cdremy@umich.edu)

not observed in human locomotion, but has been predicted through conceptual simulations [10].

II. METHODS

A. Mechanical Dynamics

The equations of motion (EOMs) are stated in a floating base description with m unilateral contact constraints (as described in [11], [12]):

$$\mathbf{M}(\mathbf{q})\ddot{\mathbf{q}} = \mathbf{h}(\mathbf{q}, \dot{\mathbf{q}}) + \boldsymbol{\tau} + \mathbf{J}^T(\mathbf{q})\boldsymbol{\lambda}. \tag{1}$$

The dynamics of this system are given by the mass matrix $\mathbf{M}$, the differentiable force vector $\mathbf{h}$ (which includes gravitational and coriolis forces), the torque vector $\boldsymbol{\tau}$, and the contact Jacobian $\mathbf{J} = \partial\boldsymbol{\phi}/\partial\mathbf{q}$ which maps a vector of contact forces $\boldsymbol{\lambda} \in \Re^{2m}$ into the generalized coordinate space.

For each unilateral constraint, the contact force $\boldsymbol{\lambda} = (\lambda_x,\ \lambda_y)^T$ and the constraint violation $\boldsymbol{\phi} = (\phi_x,\ \phi_y)^T$ are expressed in a reference frame with components that are tangent (x) and normal (y) to the contact surface. We assume that no sliding occurs in a closed contact. According to [13], the following constraints must hold for each possible contact:

$$\phi_y(\mathbf{q}) \geq 0 \tag{2}$$
$$\lambda_y \geq 0 \tag{3}$$
$$(\mu\lambda_y)^2 - \lambda_x^2 \geq 0 \tag{4}$$
$$\phi_y(\mathbf{q})\lambda_y = 0 \tag{5}$$
$$\Psi_x(\mathbf{q}, \dot{\mathbf{q}})\lambda_y = 0 \tag{6}$$

where $\boldsymbol{\Psi}(\mathbf{q}, \dot{\mathbf{q}}) = (\Psi_x\ \Psi_y)^T = \mathbf{J}\dot{\mathbf{q}}$ is the velocity of the contact point on the foot. Equations (2)-(6) are called *complementary conditions*. Eq. (2) states that a foot cannot penetrate into the ground. Eq. (3) states that normal contact force λ_y must be positive. The static friction limit (with the friction coefficient μ) is described in Equation (4). Eq. (5) ensures that the contact force can be nonzero if and only if the foot is in contact with the ground and eq. (6) states the no-slip condition. Since no friction model is included, eq. (4) could be substituted by the simpler complementary condition $\phi_y(\mathbf{q})\lambda_x = 0$, as both conditions essentially ensure that no horizontal contact force is applied when a foot is in the air. The advantage of the formulation in eq. (4) is, however, that the constraint can only be fulfilled if the lateral forces are within a permissible range. If the lateral forces become too large, the optimization cannot converge.

B. Discretization

The solution to the dynamic equations that have been stated above is usually complex, since discontinuities arise from the Coulomb friction law and from impulsive forces that occur when a contact closes. Usually, *measure differential inclusions*, which combine differential inclusions and impulsive force, are used to represent the solution of above equations [14], [15]. These problems can be avoided by solving the dynamic equation in a discrete fashion, where impact forces are averaged over an extended time step [16]. Posa and Tedrake, for example, suggest the following discretization of the EOMs [8]:

$$\begin{aligned} \mathbf{q}_{k+1} &= \mathbf{q}_k + h\dot{\mathbf{q}}_{k+1} \\ \dot{\mathbf{q}}_{k+1} &= \dot{\mathbf{q}}_k + h\mathbf{F}(\dot{\mathbf{q}}_{k+1}, \mathbf{q}_{k+1}, \mathbf{u_{k+1}}, \boldsymbol{\lambda_{k+1}}) \end{aligned} \tag{7}$$

where $\mathbf{F} = \mathbf{M}\backslash\left(\mathbf{h} + \boldsymbol{\tau} + \mathbf{J}^T\boldsymbol{\lambda}\right)$, $\mathbf{u}$ is the vector of inputs, h is the length of the time steps and $k = 1, \ldots, N-1$. $\mathbf{q}_1 = \mathbf{q}(t_o)$, $\mathbf{q}_N = \mathbf{q}(t_{end})$, and the same holds for $\mathbf{u}$ and $\boldsymbol{\lambda}$. Eq. (7) can be interpreted as a set of dynamic constraints that represent a backward Euler integration. These dynamic constraints must hold in addition to the complementary conditions of eqs. (2)–(6). To this end, their continuous form is simply modified to be fulfilled only at discrete time steps t_k. The accuracy of this approximation is $O(h)$.

Since larger time steps reduce the size of the optimization problem and increase the rate of convergence, it is highly desirable to employ higher order integration methods that have reasonable accuracy with a large time step length. Unfortunately, if no collision detection is performed, the integration method cannot exceed order one [17], [18]. Nevertheless, there is still some room for improvement since not all states are subject to discontinuities. In the following we will introduce and evaluate a modification to the discretization scheme of eq. (7) that uses a combination of trapezoidal and backward Euler integration.

Suppose a contact happens between t_k and t_{k+1}. Eqs. (5) and (6) combined with the backward Euler integration scheme imply that: $\phi_{y,k} > 0$, $\phi_{y,k+1} = 0$, $\Psi_{y,k+2} = 0$, and $\Psi_{x,k+1} = 0$. Since λ_y and λ_x can be non-zero after the collision, the impulse force drives ϕ_y and Ψ_x to zero in one step, and drives Ψ_y to zero in two steps. A trapezoidal integration scheme, for example, would additionally imply that $\Psi_{y,k+1} = 0$. That result would mean that, in the y direction, the impulsive force $\lambda_{y,k+1}$ would need to drive both position and velocity to zero within one step, which is obviously not possible.

Yet, by employing a quasi-trapezoidal integration scheme to only the velocities $\dot{\mathbf{q}}$, while using backward Euler integration for all positions $\mathbf{q}$, this problem can be circumvented. We can express such an integration scheme as:

$$\begin{aligned} \mathbf{q}_{k+1} &= \mathbf{q}_k + h\dot{\mathbf{q}}_{k+1} \\ \dot{\mathbf{q}}_{k+1} &= \dot{\mathbf{q}}_k + \frac{h}{2}(\mathbf{F}(\dot{\mathbf{q}}_{k+1}, \mathbf{q}_{k+1}, \mathbf{u_{k+1}}, \boldsymbol{\lambda}_{k+1}) \\ &\quad + \mathbf{F}(\dot{\mathbf{q}}_k, \mathbf{q}_k, \mathbf{u_k}, \boldsymbol{\lambda}_{k+1})) \end{aligned} \tag{8}$$

One can see that the integration method shown above creates the same constraint on Ψ as a backward Euler method, and that Ψ_y is still driven to zero in two steps. Note that the second equation is not a pure trapezoidal integration. We still have to use a piecewise constant function to describe the contact forces. If we use a piecewise linear function on the contact forces, eq. (3) could be violated due to the oscillation caused by trapezoidal integration.

In addition to this, we can identify a set of generalized coordinates $\bar{\mathbf{q}}$ whose velocity is always continuous with respect to time. In the proposed model, the velocity discontinuities velocities are always a result of contact collisions. To compute the instantaneous change in velocity during such a collision, the EOMs (1) are integrated over the duration of the collision.

$$\begin{aligned} \lim_{t^- \to t^+} \int_{t^-}^{t^+} \left\{\mathbf{M}\ddot{\mathbf{q}} - \mathbf{h} - \mathbf{f} - \mathbf{J}^T\boldsymbol{\lambda}\right\} dt \\ = \mathbf{M}\left(\dot{\mathbf{q}}^+ - \dot{\mathbf{q}}^-\right) - \mathbf{J}^T\boldsymbol{\Lambda} = 0 \end{aligned} \tag{9}$$

Since the integration interval is infinitesimally small, all bound forces disappear from the EOMs. Only the contact forces, which become infinitely large in the limit, contribute to the discrete changes in velocities (in an impulsive form $\mathbf{\Lambda}$). By rearranging this equation, the instantaneous velocity change can be expressed as:

$$\left(\dot{\mathbf{q}}^{+} - \dot{\mathbf{q}}^{-}\right) = \mathbf{M}^{-1}\mathbf{J}^{T}\mathbf{\Lambda} \tag{10}$$

Without knowing the exact values for the impulses $\mathbf{\Lambda}$, we can see that a generalized velocity is always continuous if all elements of the corresponding row of $\mathbf{M}^{-1}\mathbf{J}^{T}$ are equal to zero. Physically, this is the case if a segment is not rigidly connected to the remainder of the multi body system (such as the reflected inertias of SEAs), or if the contact forces are neither directly nor indirectly exerted on a degree of freedom.

For the corresponding coordinates $\bar{\mathbf{q}}$, we can switch to a higher order integration method, while the remaining coordinates $\hat{\mathbf{q}}$ are integrated with a standard backward Euler method. In combination with eq. (8), this leads to the following set of constraints:

$$\begin{aligned}
\bar{\mathbf{q}}_{k+1} &= \bar{\mathbf{q}}_k + \frac{h}{2}\left(\dot{\bar{\mathbf{q}}}_{k+1} + \dot{\bar{\mathbf{q}}}_k\right) \\
\hat{\mathbf{q}}_{k+1} &= \hat{\mathbf{q}}_k + h\dot{\hat{\mathbf{q}}}_{k+1} \\
\dot{\bar{\mathbf{q}}}_{k+1} &= \dot{\bar{\mathbf{q}}}_k + \frac{h}{2}(\mathbf{F}\left(\dot{\mathbf{q}}_{k+1}, \mathbf{q}_{k+1}, \mathbf{u_{k+1}}, \boldsymbol{\lambda}_{k+1}\right) \\
&\qquad + \mathbf{F}\left(\dot{\mathbf{q}}_k, \mathbf{q}_k, \mathbf{u_k}, \boldsymbol{\lambda}_k\right)) \\
\dot{\hat{\mathbf{q}}}_{k+1} &= \dot{\hat{\mathbf{q}}}_k + \frac{h}{2}(\mathbf{F}\left(\dot{\mathbf{q}}_{k+1}, \mathbf{q}_{k+1}, \mathbf{u_{k+1}}, \boldsymbol{\lambda}_{k+1}\right) \\
&\qquad + \mathbf{F}\left(\dot{\mathbf{q}}_k, \mathbf{q}_k, \mathbf{u_k}, \boldsymbol{\lambda}_{k+1}\right))
\end{aligned} \tag{11}$$

Since some states are still integrated by the backward Euler method, the overall order of accuracy remains $O(h)$ in theory. Nevertheless, in practical implementations, the partial trapezoidal method introduces considerable improvements.

C. Optimization

The aforementioned discrete dynamic formulation can be used as a set of nonlinear constraints in an optimal control problem. Since we are particularly interested in identifying energy efficient gaits, we will minimize a cost function that expresses the cost of transport (COT) [19]; that is, the amount of energy used per distance traveled. Specifically, we will focus on the positive mechanical joint work

$$W = \int_{t_o}^{t_{end}} \sum_{i=1}^{p} \max\left(\tau_i \dot{u}_i, 0\right)\, dt \tag{12}$$

which is computed from the positive mechanical power of p joints and integrated over the duration of a stride (t_o - t_{end}). The COT is:

$$C = W / \left(x\left(t_{end}\right) - x\left(t_o\right)\right) \tag{13}$$

In a time discrete model with backward Euler integration, this positive mechanical joint work can be expressed as the sum:

$$W = h \sum_{k=2}^{N} \sum_{i=1}^{p} \max\left(\tau_{i,k} \dot{u}_{i,k}, 0\right) \tag{14}$$

and the COT as:

$$W = h \sum_{k=2}^{N} \sum_{i=1}^{p} \max\left(\tau_{i,k} \dot{u}_{i,k}, 0\right) / \left(x_N - x_1\right) \tag{15}$$

TABLE I

MODEL PARAMETERS EXPRESSED WITH RESPECT TO TOTAL MASS m_o, LEG LENGTH l_o, AND GRAVITY g.

m_1 = 0.7 m_o	j_2 = 0.002 $m_o l_o^2$	r_{foot} = 0.05 l_o
m_2 = 0.1 m_o	j_3 = 0.002 $m_o l_o^2$	k_l = 10 $m_o g / l_o$
m_3 = 0.05 m_o	j_α = 0.016 $m_o l_o^2$	ζ_l = 0.2
m_l = 1.0 m_o	l_2 = 0.25 l_o	k_α = 5 $m_o g l_o / rad$
j_1 = 0.4 $m_o l_o^2$	l_3 = 0.25 l_o	ζ_α = 0.2

While using trapezoidal integration to discretize the cost function is possible for some models, it might contaminate the stability of the optimizer in most cases.

With this, the search for an optimal gait can be expressed as the constrained nonlinear optimization problem

$$\begin{aligned}
&\min\left(C\right) \\
&h, \mathbf{q}_1, \ldots, \mathbf{q}_N, \mathbf{u}_1, \ldots, \mathbf{u}_N, \boldsymbol{\lambda}_1, \ldots, \boldsymbol{\lambda}_N
\end{aligned} \tag{16}$$

subject to equation (11), the discrete form of the complimentary conditions (2)-(6), and additional boundary conditions on $\mathbf{q}\left(t_o\right)$ and $\mathbf{q}\left(t_{end}\right)$. Further constraints can reflect, –for example– physical limitations of the actuators or enforce a desired average locomotion velocity. One important characteristic of this method is that the contact forces are treated as free variables instead of being solved at each step.

D. Model

Since the models used in this study (Fig. 1) have already been presented elsewhere (e.g., [20]), we will merely highlight some of their key features: They have a main body with mass m_1 and rotational inertia j_1, two upper leg segments (m_2, j_2), and two lower leg segments (m_3, j_3). The position and orientation of the main body is given by (x, y, ϕ). Main body and upper legs are connected by rotational hip joints (with joint-angle $\alpha_{L/R}$), and the two leg segments in each leg are connected prismatically (the resulting leg length $l_{L/R}$ is measured from the hip to the foot-center).

In the joints, the motion of two adjoining segments is coupled by linear springs with stiffness $k_l\left(k_\alpha\right)$ and damping ratio $\zeta_l\left(\zeta_\alpha\right)$. These springs are rigidly attached to the distal segments and, on the other side, connected to electrical servo-controlled motors with motor displacements of $u_{lL/R}\left(u_{\alpha L/R}\right)$. Joint, motor, and spring form a Series Elastic Actuator (SEA [21]). The motors have a reflective inertia of m_l (j_α). Having damping in the springs and a mass associated with the foot means that the system is energetically not conservative and that positive net work must be performed by the actuators over the course of a stride.

The vector of generalized coordinates is defined by $\mathbf{q} = \left(x,\ y,\ \varphi,\ \alpha_L,\ l_L,\ \alpha_R,\ l_R,\ u_{\alpha L},\ u_{lL},\ u_{\alpha R},\ u_{lR}\right)^T$. All states and parameters are normalized with respect to total mass m_o, uncompressed leg length l_o, and gravity g (Table I). The model is driven by the actuator torques $\mathbf{u} = \left(\tau_{\alpha L},\ \tau_{lR},\ \tau_{\alpha R}\right)^T$. Joint forces are computed by:

$$\begin{aligned}
F_{lL/R} &= k_l\left(l_o + u_{lL/R} - l_{L/R}\right) + b_l\left(\dot{u}_{lL/lR} - \dot{l}_{L/R}\right) \\
T_{\alpha L/R} &= k_\alpha\left(\alpha_o + u_{\alpha L/R} - \alpha_{L/R}\right) + b_\alpha\left(\dot{u}_{\alpha L/R} - \dot{\alpha}_{L/R}\right)
\end{aligned} \tag{17}$$

The damping coefficients $b_l\,(b_\alpha)$ are computed from desired damping ratios $\zeta_l\,(\zeta_\alpha)$. The generalized torques are given as $\tau = (0,\ 0,\ 0,\ T_{\alpha L},\ F_{lL},\ T_{\alpha R},\ F_{lR},\ \tau_{\alpha L},\ \tau_{lL},\ \tau_{\alpha R},\ \tau_{lR})^T$. Initially, the motion of the model will be simplified to one dimensional hopping. The simplified model (Fig. 1b) has only one leg, with x, φ, α fixed at zero. With this simplification, the main body and the upper leg can be lumped together: $m_{mb} = m_1 + m_2$, and the number of degrees of freedom (DoF) is reduced from eleven to three ($\mathbf{q} = (y,\ l,\ u_l)^T$) and the number of actuators from four to one ($\mathbf{u} = \tau_l$). Moreover, since there is no tangential motion between the foot and the ground, the complementary constraints are greatly simplified. This 1D model is thus a good starting point to analyze the stability, accuracy and robustness of the proposed method.

For the 2D model, the positive mechanical joint work can be expressed as

$$W = \int_{t_o}^{t_{end}} \max\left(\tau_{lL}\dot{u}_{lL}, 0\right) + \max\left(\tau_{\alpha L}\dot{u}_{\alpha L}, 0\right) + \max\left(\tau_{lR}\dot{u}_{lR}, 0\right) + \max\left(\tau_{\alpha R}\dot{u}_{\alpha R}, 0\right)\ dt$$

and the COT C computed according to eq. (13) Since there is no forward motion in the 1D model, the cost function for this model is not expressed via the COT, but via the positive mechanical joint work:

$$C = W = \int_{t_o}^{t_{end}} \max\left(\tau_l \dot{u}_l, 0\right)\ dt \tag{18}$$

E. Implementation

To evaluate the proposed method, we implemented both, pure backward Euler integration using the constraints of eq. (7), and the proposed partial trapezoidal integration using the constraints of eq. (11). The resulting nonlinear constraint optimization problem was implemented and solved with the MATLAB optimization toolbox [22]. The number of time grid points used in this paper was around 50, similar to comparable studies [8], [13]. Additionally, the results were compared to motions optimized via an established multiple shooting framework that relies on an a-priory defined contact sequence. (MUSCOD [23]).

III. RESULTS

A. 1D Model, Passive

As an introductory example and general proof of concept we evaluated the proposed method in a fully passive 1D model. To this end, the actuator position u_l was constrained to a constant value of zero. Without actuation, there is no joint power and the cost function $C \equiv 0$. Rather than solving an optimization, we are thus merely finding a solution that fulfills the dynamic constraints; that is, the optimization problem is reduced to a pure forward dynamic simulation. The initial states for this simulation are set to be $y\,(t_o) = 1.3\,\mathrm{l_o}$, $\dot{y}\,(t_o) = 0$, $l\,(t_o) = 1\,\mathrm{l_o}$ and $\dot{l}\,(t_o) = 0$. For the resulting bouncing motion, an analytic solution can be computed as reference.

A standard backward Euler integration scheme (eq. (7)) converges reliably and shows good numerical stability, even under large time-steps. As the step size decreases, motion trajectories converge towards the analytic solution (Fig. 2). The convergence of this method is proven in [24] and the numerical stability is guaranteed.

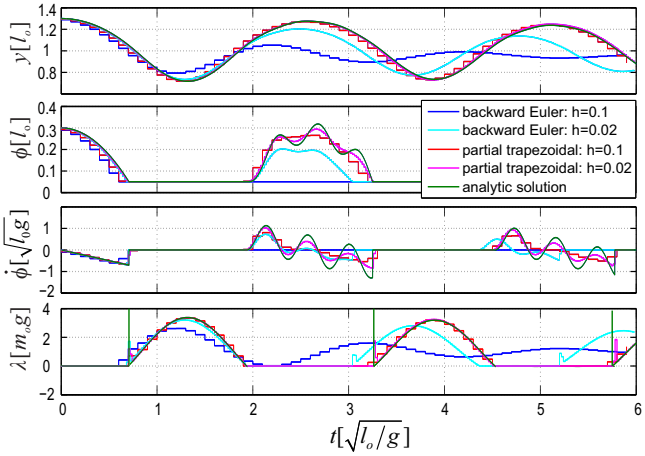

Fig. 2. Motion trajectories of an unactuated 1D hopper are compared to an analytic solution for the two different methods and for different time step lengths h. Shown are: the vertical position of the main body y, the vertical position ϕ of the feet, the vertical velocity $\dot{\phi}$ of the feet, and the vertical contact forces between the feet and the ground λ.

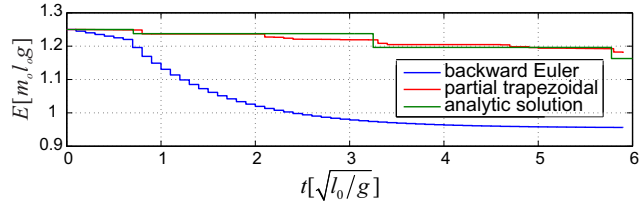

Fig. 3. Total system energy of an unactuated 1D hopper is shown with respect to time. Since in this case no damping was assumed for the leg spring, the analytic solution shows that the total system energy is constant except during collisions. Due to numerical 'damping', almost 20 % of the system energy is erroneous lost with a pure backward Euler integration. In contrast, our proposed improvements very closely match the true energetics. A time step of $h = 0.1$ was used for this simulation.

However, even for a very small time step h, a notable loss in system energy becomes apparent when comparing the results with the analytic solution. This loss can be seen clearly in Fig. 3. Since in this particular example the damping ratio ζ was set to 0, the total energy of the system is expected to remain constant between collisions. With the backward Euler approach, about 20 % of the total system energy is dissipated during flight and stance. This energy loss is caused by the nature of the implicit Euler integration method. As shown in [24], the backward Euler integration method is energetically non-increasing. For large h, the inaccuracy of each step will result in an accumulated energy loss.

In order to improve the accuracy, we can identify a set of generalized coordinates $\bar{\mathbf{q}}$ that are not subject to discontinuous changes in velocity. For this model, the mass matrix $\mathbf{M}$ and the contact Jacobian $\mathbf{J}$ are given by

$$\mathbf{M} = \begin{pmatrix} m_{mb}+m_3 & -m_3 & 0 \\ -m_3 & m_3 & 0 \\ 0 & 0 & m_r \end{pmatrix} \text{ and } \mathbf{J^T} = \begin{pmatrix} 1 \\ -1 \\ 0 \end{pmatrix},$$

and we get

$$\mathbf{M^{-1}J^T} = (0, -1/m3, 0)^T\,.$$

The above equation shows that only $\dot{l}$ is subject to discontinuities. Motor, main body, and foot are decoupled by the series elastic element, such that the impact forces acting on the foot are not passed onto the motor and main body. The velocity of the main body $\dot{y}$ and actuator $\dot{u}_l$ will remain continuous in the event of a collision. Using trapezoidal integration for these continuous states leads to a tremendous improvement in energetic accuracy. Since the main body contains 95 % of the total mass and the foot stays on the ground for about half the time, the movement of the main body determines a large part of the dynamic behavior of the system. By applying a higher order integration method to this part of the dynamics, the accuracy of the solution is greatly improved. In a similar manner, we implemented dynamic constraints, in which velocities were calculated based on a trapezoidal integration scheme and positions were based on a backward Euler integration. With these changes, l is the only dynamic state that is computed via backward Euler integration. y, u_l, and all velocities are computed via trapezoidal integration. This method is stable for time steps up to $h = 0.5$. A solution with $h = 0.1$ is nearly identical to the analytic solution, both in terms of motion trajectories and in terms of the predicted energy loss.

B. 1D Model, Active

By adding actuation to the 1D Model and by enforcing periodicity over multiple cycles, a true optimal control problem is created. The simulation is started and terminated at apex transit (i.e., when the vertical velocity $\dot{y}$ is zero) and periodic boundary conditions are enforced via the following constraints: $\mathbf{q}(t_o) = \mathbf{q}(t_{end})$ and $\dot{\mathbf{q}}(t_o) = \dot{\mathbf{q}}(t_{end})$. We created two slightly different variations of this problem: In the first variation, we fully specified the physical states at apex transit by setting $y(t_o) = 1.3\,\mathrm{l_o}$, $\dot{y}(t_o) = 0$, $l(t_o) = 1.0\,\mathrm{l_o}$, and $\dot{l}(t_o) = 0$. In the second variation, only the height of apex transit was defined ($y(t_o) = 1.3\,\mathrm{l_o}$. $\dot{y}(t_o) = 0$), while $l(t_o)$ and $\dot{l}(t_o)$ were chosen by the optimizer. In both variations, the actuator position $u_l(t_o)$ and velocity $\dot{u}_l(t_o)$ at apex transit were not specified.

The small difference between the two variations has a huge impact on the structure of the expected solution. While in the first case, the model is required to perform a true hopping motion and lift the foot off the ground during apex transit, no such requirement exists in the second variation. The best solution for the latter case is consequently that the 1D hopper stands still with its leg extended to $l = 1.25\,\mathrm{l_o}$ ($r_{foot} = 0.05\,\mathrm{l_o}$). To achieve this, the actuator can simply remain at rest at $u_l = 0.25\,\mathrm{l_o} + \frac{mg}{k}$. Since all states are constant in the latter case, the stride period t_{end} is not strictly defined. No energy is lost or replaced in the process. Similarly, we can make predictions about the solution of the first case [20].

Optimal trajectories are shown for the two different boundary conditions in Fig. 4. The solution closely matches the predictions stated above. If a true hopping motion is enforced, the actuator remains motionless for the first half of stance to avoid negative work and keep P_{damp} small. Throughout the second half of stance, when the leg is extending, the actuator is extending as well, trying to keep $(\dot{l} - \dot{u}_l)^2$ and thus the damping power P_{damp} small. If the leg length was not constrained during apex transit, the optimization converged to the expected static solution with an actuator that is at rest. Note, that the latter result might not be found by an optimal control method that requires an a-priory defined contact sequence and that would strictly enforce an air-phase.

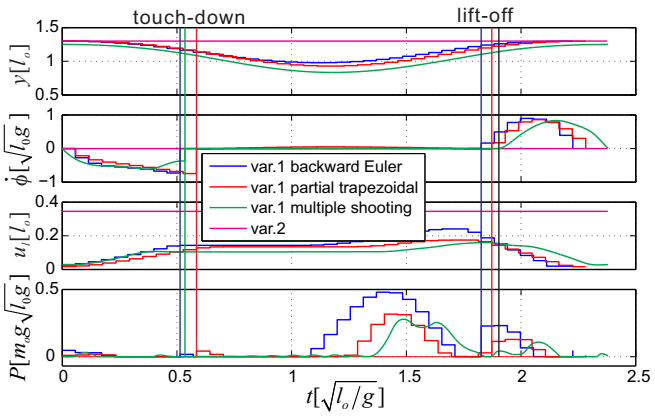

Fig. 4. Optimization results of two variations of a 1D hopping motion. Enforcing a leg length of $l = 1\,\mathrm{l_o}$ at the boundary condition requires an actual hopping motion (Var. 1). If this constraint is not enforced (Var. 2), the optimal result keeps all states constant and no energy is put into the system. Optimizations were performed for 40 grid points.

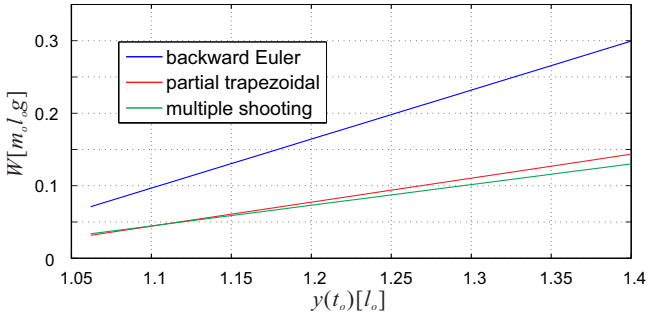

Fig. 5. The positive mechanical actuator work of in-place hopping is shown for a varying hopping height $y(t_o)$. Three different optimization methods are compared for an optimization with 40 grid points. While a pure backward Euler integration overpredicts energy consumption by as much as 100 %, cost values found by our modified method are very close to the results obtained by multiple shooting.

Optimal trajectories that we obtained by using different time discretization methods were similar in shape, but differed greatly in the amount of predicted energy consumption. Figure 5 shows the values of positive mechanical joint work as a function of hopping height $y(t_o)$ and compares them to solutions found via multiple shooting. While a pure backward Euler integration overpredicts energy consumption by as much as 100 %, cost values found by our modified method are very close to the results obtained by multiple shooting.

C. Bipedal Robot

Finally, we applied our proposed method to the model of a planar bipedal robot and identified optimal gaits and motions for varying locomotion speeds. We only considered steady-state forward motion; i.e., all states of the system were

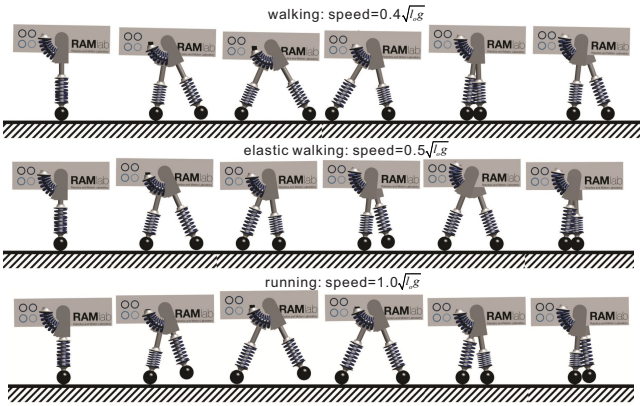

Fig. 6. Motion frames of the bipedal robot moving at three different locomotion speeds. As speed is increased, the optimal solution changes from walking, to an elastic walking gait, and then to running. All gaits are also included in the video attachment of this paper.

enforced to be periodic, except the horizontal position x. Optimizations were performed to minimize the mechanical COT. Since the model is symmetric, we restricted the optimization to a half-stride, which greatly reduced the scale of the optimization problem. In order to define boundary conditions that are not over restricting the motion, we chose $\alpha_L(t_{end}) = \alpha_R(t_{end})$ to define the end of a stride. An evaluation of $\mathbf{M^{-1}J^T}$ shows that the following coordinates are continuous during collisions, and can thus be integrated via trapezoidal integration: ϕ , $u_{\alpha L}$, u_{lL} , $u_{\alpha R}$ and u_{lR}. All motor states are decoupled from the rest of the model in the mass matrix and the corresponding columns in the contact Jacobian are zero. Since the main body is connected with the two legs at the COG, no impulsive torques from contact collisions act on the main body. So $\dot{\phi}$ is continuous.

The structure of the solution and the order of contact events vary as locomotion velocity is increased. For slow velocities ($< 0.55\sqrt{l_o g}$), the optimizer identifies walking as the optimal motion (Fig. 6 top). At slow speeds, the leg springs undergo two full compression cycles during stance. These cycles lead to a characteristic double hump that can be observed in the vertical ground reaction forces, similar to human walking [25] (Fig. 7 top). If the velocity is increased, the order of the footfall sequence remains the same, but the pattern of the ground reaction forces changes dramatically. A single hump in vertical ground reaction forces indicates that the leg spring is only undergoing a single compression during stance. This 'elastic walking gait' is also characterized by a very short phase of double support (Figs. 6 and 7 center). If the locomotion velocity is increased beyond $0.75\sqrt{l_o g}$, the order of contact changes. Lift-off of the left foot happens before touchdown of the right foot, and an substantial air-phase is introduced (Figs. 6 and 7 bottom).

The different gaits were detected automatically and are –together with the detailed motion trajectories– a result of the optimization process. Figure 9 shows how the time of double support decreases as locomotion speed is increasing and highlights how a nearly instantaneous change of support is sought at intermediate velocities. Notably, the transition

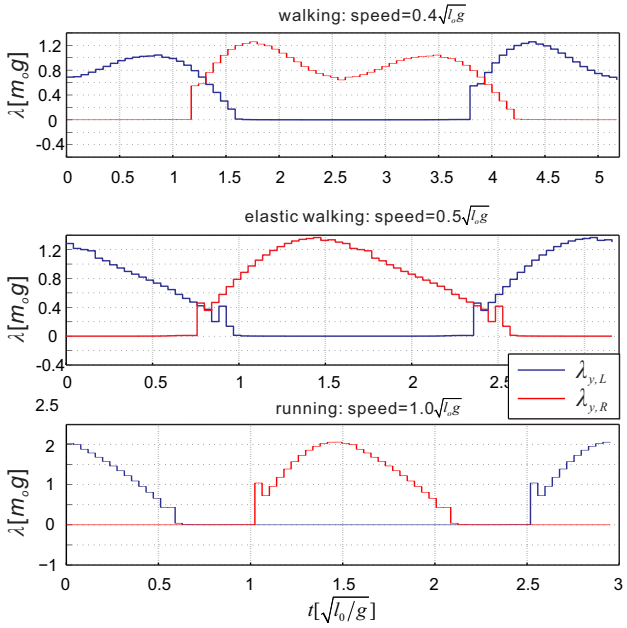

Fig. 7. Vertical contact forces as a function of time for three different locomotion speeds. This data was obtained via the proposed partial trapezoidal integration. Optimization was performed for 40 grid points.

to running with an extended air phase happens almost instantaneously and the duration of the air phase is not increased incrementally. The only notable difference between the solutions obtained via the proposed collocation approach and the solution that we obtained via multiple shooting is the duration of this air-phase. We hypothesize that the numerical damping that originates in the backward Euler integration penalizes an extended air phase that is nearly free from loses in the physical world. While the effect impacts both, the original method and the partial trapezoidal integration, the latter still reduces the error in energetic prediction by about 50 %.

Finally, the energetic benefits of employing different gaits as locomotion velocity changes, can be seen clearly in Fig. 8 which shows the COT as a function of speed. Comparing the results with multiple shooting solutions of two different gaits shows that at different velocities, different contact sequences are energetically more efficient. Restricting the contact sequence, and thus the gait a-priory, would nearly double the COT for very slow running, or very fast walking.

IV. CONCLUSION AND FUTURE WORK

This paper introduced an improvement to an optimal control approach for hybrid systems that does not rely on an a-priori defined contact sequence. To this end, we systematically identified states that are continuous during collisions and applied a higher order integration scheme to these. We evaluated the proposed method with models of a 1D hopper and a bipedal robot. While, in theory, the accuracy of the proposed method is still $O(h)$, we could show that it leads to a substantial performance improvement in practical implementation.

With the proposed changes, we are able to simultaneously identify motions and gaits for legged robotic systems.

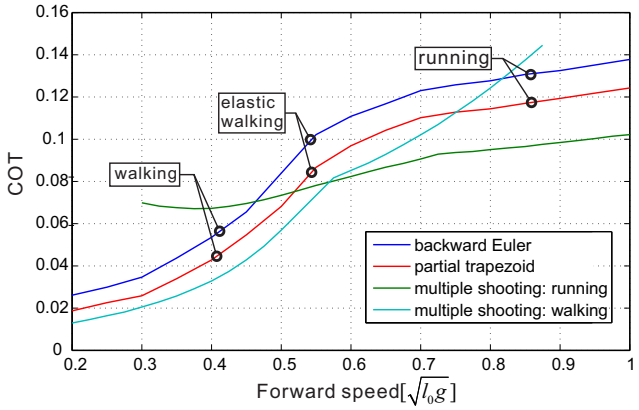

Fig. 8. The cost of transportation (COT) is shown in respect to locomotion speed for the different methods. At low speeds, walking is the most efficient gait. At high speeds $(> 0.55\sqrt{l_o g})$, running is the optimal gait. In between an elastic walking gait is found.

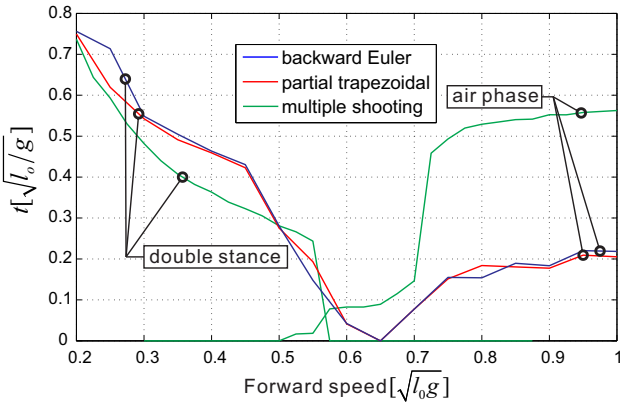

Fig. 9. The duration of double support during walking and the duration of the air phase during running are shown as a function of speed for the different optimization techniques.

In the bipedal model, our optimal control approach was able to predict a gait transition from walking to running as locomotion velocity was increased. Similar to human locomotion, the COT of such an SEA driven robot could be minimized by switching from one contact sequence to another. Furthermore, an elastic walking gait was discovered, which –although not present in human locomotion– increased the energetic efficiency of our bipedal model.

All motions that we discovered fully exploit the *natural dynamics* of the mechanical systems and can be interpreted as complex nonlinear oscillations which are merely excited and maintained through periodic actuator inputs. The different gaits that we identified correspond to a variety of discrete modes in which these natural dynamics can be excited. This phenomenon could be observed most clearly when comparing walking gaits at slow speeds with the elastic walking gaits at medium speeds. In one gait, the leg springs undergo a single oscillation, while in the other, two oscillations. To further investigate the exploitation of natural dynamics, we will extend such conceptual studies to quadrupedal locomotion. Quadrupeds are particularly interesting, since they allow for a much broader variety of possible contact sequences. While there is a certain expectation that gaits that are used in nature (such as walking, trotting, or galloping) will also prove to be useful in robotics, our proposed method will enable us to answer this question based on first principles.

REFERENCES

[1] J. T. Betts, *Practical methods for optimal control and estimation using nonlinear programming*, vol. 19. Siam, 2010.

[2] C. Hargraves, "Direct trajectory optimization using nonlinear programming and collocation," *Journal of Guidance Control, and Dynamics*, pp. 10–4, 1987.

[3] O. von Stryk and R. Bulirsch, "Direct and indirect methods for trajectory optimization," *Annals of Operations Research*, vol. 37, no. 1, pp. 357–373, 1992.

[4] A. David, "Winter. biomechanics and motor control of human movement," *Wiley,*, vol. 6, p. 1, 1990.

[5] C. D. Remy, *Optimal Exploitation of Natural Dynamics in Legged Locomotion*. PhD thesis, Eidgenssische Technische Hochschule, 2011.

[6] R. Goebel, R. G. Sanfelice, and A. Teel, "Hybrid dynamical systems," *Control Systems, IEEE*, vol. 29, no. 2, pp. 28–93, 2009.

[7] G. Schultz and K. Mombaur, "Modeling and optimal control of human-like running," *Mechatronics, IEEE/ASME Trans. on*, vol. 15, no. 5, pp. 783–792, 2010.

[8] M. Posa and R. Tedrake, "Direct trajectory optimization of rigid body dynamical systems through contact," in *Algorithmic Foundations of Robotics X*, pp. 527–542, Springer, 2013.

[9] I. Mordatch, J. M. Wang, E. Todorov, and V. Koltun, "Animating human lower limbs using contact-invariant optimization," *ACM Transactions on Graphics (TOG)*, vol. 32, no. 6, p. 203, 2013.

[10] M. Srinivasan and A. Ruina, "Computer optimization of a minimal biped model discovers walking and running," *Nature*, vol. 439, no. 7072, pp. 72–75, 2006. 10.1038/nature04113.

[11] M. Anitescu and F. A. Potra, "Formulating dynamic multi-rigid-body contact problems with friction as solvable linear complementarity problems," *Nonlinear Dynamics*, vol. 14, no. 3, pp. 231–247, 1997.

[12] K. D. Bhalerao, C. Crean, and K. Anderson, "Hybrid complementarity formulations for robotics applications," *ZAMM-Journal of Applied Mathematics and Mechanics*, vol. 91, no. 5, pp. 386–399, 2011.

[13] M. Posa, C. Cantu, and R. Tedrake, "A direct method for trajectory optimization of rigid bodies through contact," 2012.

[14] J. J. Moreau, "Standard inelastic shocks and the dynamics of unilateral constraints," *Unilateral problems in structural analysis*, no. 288, pp. 173–221, 1983.

[15] D. E. Stewart, "Rigid-body dynamics with friction and impact," *SIAM review*, vol. 42, no. 1, pp. 3–39, 2000.

[16] D. Stewart and J. Trinkle, "An implicit time-stepping scheme for rigid body dynamics with inelastic collisions and coulomb friction," *Int. J. for Numerical Methods in Engineering*, vol. 39, 1996.

[17] M. Anitescu, "A fixed time-step approach for multibody dynamics with contact and friction," in *Intelligent Robots and Systems, IEEE/RSJ International Conference on*, vol. 4, pp. 3725–3731, IEEE, 2003.

[18] E. Hairer, "N rsett, sp, wanner, g., solving ordinary differential equations, i," *Nonstiff Problems, Springer Series in Compmotional Mathematics*, vol. 8, 1987.

[19] V. A. Tucker, "The energetic cost of moving about: Walking and running are extremely inefficient forms of locomotion. much greater efficiency is achieved by birds, fishand bicyclists," *American Scientist*, vol. 63, no. 4, pp. 413–419, 1975.

[20] C. Remy, K. Buffinton, and R. Siegwart, "Comparison of cost functions for electrically driven running robots," 2012.

[21] M. Hutter, C. D. Remy, and R. Siegwart, "Design of an articulated robotic leg with nonlinear series elastic actuation," in *International Conference on Climbing and Walking Robots CLAWAR*, 2009.

[22] M. O. Toolbox, "The mathworks," *Inc. Natick, MA*, 2001.

[23] M. Diehl, D. B. Leineweber, and A. A. Schäfer, *MUSCOD-II User's Manual*. IWR, 2001.

[24] D. E. Stewart, "Convergence of a time-stepping scheme for rigid-body dynamics and resolution of painlevé's problem," *Archive for Rational Mechanics and Analysis*, vol. 145, no. 3, pp. 215–260, 1998.

[25] D. A. Winter, *Biomechanics and motor control of human movement*. Wiley. com, 2009.